

Intelligent structural defect reconstruction using the fusion of multi-frequency and multi-mode acoustic data

Qi Li¹, Hairui Liu¹, Peng Li¹, Shirsendu Sikdar², Bin Wang¹, Zhenghua Qian^{1,*}, Dianzi Liu^{3,*}

¹*State Key Laboratory of Mechanics and Control of Mechanical Structures, College of Aerospace Engineering, Nanjing University of Aeronautics and Astronautics, Nanjing, 210016, China*

²*School of Engineering, Cardiff University, UK*

³*School of Engineering, University of East Anglia, UK*

* Corresponding authors, E-mail: dianzi.liu@uea.ac.uk; qianzh@nuaa.edu.cn.

Abstract:

Quantitative detection of defects in structures is always a hot research topic in the field of guided wave inverse scattering. Research studies on how to effectively extract the defect-related information encompassed in the multi-frequency and multi-modes scattered wave signals for reconstructions of defects have been paid attention in recent decades. In this paper, a novel deep learning-based quantitative guided wave inverse scattering technique has been proposed to intelligently realize the end-to-end mapping of the multi-frequency, multi-modes scattered signals to defect profiles with high levels of accuracy and efficiency. Based on the manifold distribution principle, the data patterns of scattered SH-wave signals have been investigated, owing to leveraging the capability of the intelligent encoder-projection-decoder neural network. Following that, the manifold-learning oriented network has been trained using the data generated by the modified boundary element method. Several numerical examples have been examined to demonstrate the correctness and efficiency of the proposed reconstruction approach. It has been concluded that this novel data-driven technique intelligently enables the high-quality solution to inverse scattering problems and provides a valuable insight into the development of practical approaches to quantitative detection using multi-frequency and multi-modal acoustic data from scattered ultrasonic guided waves.

Keywords:

Guided wave; Inverse scattering problem; Multi-frequency; Multi-modes; Deep learning

1. Introduction

Ultrasonic guided wave testing (UGWT) is a specific inspection technique of long-standing interest due to the ability of guided waves to travel long distances with little attenuation and the high sensitivity to structural defects^[1,2]. Despite a great deal of progress on the subject of UGWT, many methods currently available are only capable of providing a qualitative assessment of structural defects^[3,4]. Consequently, the inverse scattering problem, focusing on quantitative determination of the defect shape and size in the use of various reflection and transmission signals of ultrasonic guided waves, is always a hot research topic in the field of UGWT^[5-7].

The ultrasonic array, one of the effective quantitative UGWT technology, has superior features including the large scanning range and high detection accuracy^[8]. In

earlier ultrasonic array work by Hutchins^[9,10], Achenbach^[11], and Degetekin^[12], a parallel projection technique with the velocity and attenuation of Lamb waves as the input was developed for the tomographic reconstruction. Following that, James et al^[13] presented a new Lamb wave array technique in which two contacted piezoelectric transducers were independently used for the scan along parallel lines. They applied the filtered back projection (FBP) algorithm to obtain defect images in plate like structures. Subsequently, iterative reconstruction procedures incorporated with the scattered guided waves of defects were extended to improve image quality by Malyarenko and Hinders^[14]. On the other hand, the ultrasonic array used with non-contact transducers was studied by Hay et al^[14]. The probabilistic reconstruction technique^[15] used a damage index based on the correlation of the signals before and after damage. A series of ellipses that located away from the direct line of sight were weighted by the damage index for the construction with a rapidly decreasing probability. In^[16], the guided wave tomography of a steel plate like structures with a corrosion defect was studied under the water loading conditions. Also, the omnidirectional excitation of desired guided wave modes by annular array transducers was discussed. Results showed that the defects in the structures can be easily discriminated from any artifacts in the images due to the liquid layer. In^[17], the quantitative defect sizing and imaging was achieved using the variable shape factor defined in the PAPID algorithm. With a 32-transducer network system, the location and quantitative size of complex shape defects in plate-like structures were evaluated. Xiang et al^[18] developed a sparse array ultrasonic guided wave imaging technique and proposed a quantitative defect recognition method based on the sparse scattering information extracted from the scattering coefficient matrix. They also analyzed the relationship between the sparse and full scattering coefficient matrices. In^[19], a quantitative method for evaluating the sizes of defects was proposed to assess multilayered bonded composites using the laser ultrasonic guided waves. More recently, Hashen et al^[4] developed a quantitative defect inspection technique for the structural health monitoring of curved composite structures. Based on the fusion of the modified probabilistic tomography (MPT) and the damage index (DI), the defect zones in a curved composite structure were quantitatively detected. Although the techniques aforementioned have been proven as a promising tool for the quantitative guided wave inverse scattering problems, there are still some limitations in such single-frequency tomography approaches. First, the ability of the transducer array-based techniques to fully characterize damage is weakened by the amount of defect-relate information that could be obtained through a sparse transducer array in a cost-effective manner. Second, the transducer arrangement may be not achievable in some harsh environments including the high temperature and nuclear radiation conditions. Finally, these techniques mainly make use of the time of flight (TOF) of scattered wave signals, thus they can only identify the location of defects, but fail to depict the detail of shapes.

Taking into account these facts, some researchers have investigated quantitative guided wave inverse scattering techniques using multi-frequency or multi-modal scattered wave signals containing the sufficient defect-relate information. With the integration of Green's function and Born approximation, Wang et al proposed a new method for quantitative shape reconstruction of the local thinning in the use of

reflection coefficients of guided SH-waves^[20] and Lamb waves^[21]. The depth of the plate thinning was obtained as a function of reflection coefficients at various frequencies by the inverse Fourier transform. Gregory et al^[22] developed a multi-wave-mode, multi-frequency detector for guided wave interrogation of plate structures. Experimental results showed that a single-mode, multi-frequency detector has the best detection and localization performance for the tested damage scenarios. In^[23], a new methodology based on multi-frequency local wavenumber analysis for the quantitative assessment of multi-ply delamination damages in carbon fiber reinforced polymer (CFRP) composite specimens was proposed. Simultaneously, Jennifer et al^[24] utilized a chirp function to excite PZT transducers over a broad frequency range to acquire multi-modal data with a single transmission. Each received signal from a chirp excitation was post-processed to obtain multiple signals corresponding to different narrowband frequency ranges. Recently, Da et al^[25] proposed a novel approach called as Quantitative Detection of Fourier Transform (QDFT) for efficiently detecting defects in pipeline structures. Daniel et al^[26] introduced a multi-mode and multi-frequency method for the characterization of stiffener bonded lines using Semi-Analytical Finite Element (SAFE). Gao et al^[27] presented an inspection methodology based on the multi-frequency local wavenumber estimation for quantitative assessment of hidden corrosion in plates. The methodology was verified on the aluminum plates of 1 mm thickness with the corrosion, and the relative errors between the estimated and actual value of the corrosion depth were not more than 6%.

Using information from multi-frequency and multi-wave modes to detect damage in structures requires the wave propagation knowledge e.g., the dispersion and mode conversion, in conjunction with a reconstruction algorithm that utilizes the multiple modal information in the presence of inevitable noise or uncertainty. In contrast to conventional model-based approaches, data-driven techniques, particularly Deep Learning (DL), are increasingly widely developed to solve the inverse scattering problems^[6,28], such as X-ray computed tomography imaging (CT)^[29], magnetic resonance imaging (MRI)^[30], positron emission tomography (PET)^[31] as well as ultrasonic guided wave testing (UGWT)^[32]. Through data training, these techniques can effectively extract the defect-related information from raw noise containing the scattering signals and quantitatively reconstruct the details of defect shapes.

This paper investigates the implementation of deep neural network (DNN) for quantitatively defect reconstruction of plate-like structures using guided SH-waves. Details of this research consist of three steps: First, the distribution characteristics of multi-wave modes, multi-frequency scattered signals in manifold space have been explored. Then, a novel encoder-projection-decoder neural network has been proposed to realize an end-to-end mapping from the scattered signals in the wavenumber field to the defect shapes in the spatial space. Finally, a modified boundary element method has been developed to generate the scattered signals, for example reflection coefficients, as the network input for the training purpose, leading to the reconstruction of defects with high levels of accuracy and reliability. Throughout several examples, the correctness and efficiency of the proposed quantitative inverse scattering method have been demonstrated.

2. Methodology

2.1 Background of the guided SH-wave theory

A shear horizontal (SH) wave propagating along a homogeneous, isotropic, elastic plate with the thickness of $2h$ is considered in Fig.1, where the wave propagates along the x_1 direction and the particles in the plate vibrate in the x_3 direction. The displacement field \mathbf{u} of the particle must satisfy Navier's displacement equations of the motion defined in Eq.1:

$$\mu \nabla^2 \mathbf{u} + (\lambda + \mu) \nabla \nabla \cdot \mathbf{u} - \rho \frac{\partial^2 \mathbf{u}}{\partial t^2} = 0 \quad (1)$$

Also, the traction-free boundary conditions applied to solve Eq.1 are expressed as:

$$\tau_{23}(x_1, x_2, t)|_{x_2=\pm h} = \mu \frac{\partial u}{\partial x_2} |_{x_2=\pm h} = 0 \quad (2)$$

where ρ is the mass density; λ and μ are Lamé constants. As only the component u_3 of the particle displacement field \mathbf{u} is nonzero, a time-harmonic SH-wave is formulated as

$$u_3(x_1, x_2, t) = f(x_2) e^{i(kx_1 - \omega t)} \quad (3)$$

where k is the wavenumber of the mode and ω represents the natural circular frequency. Substituting Eqs.(2-3) into Eq.(1), the dispersion equation of guided SH-waves can be deduced in a function of the wave velocity and frequency:

$$\frac{\omega^2}{c_T^2} - \frac{\omega^2}{c_p^2} = \left(\frac{n\pi}{2h} \right)^2, \quad n = 0, 1, 2, \dots \quad (4)$$

where $c_T = \sqrt{\mu/\rho}$ is the velocity of SH-wave and c_p is the phase velocity. As an example, the relationship between the phase velocities and frequencies over a range of 0-14 MHz-mm is investigated by dispersion curves for the first eight of SH waves modes shown in Fig.1b.

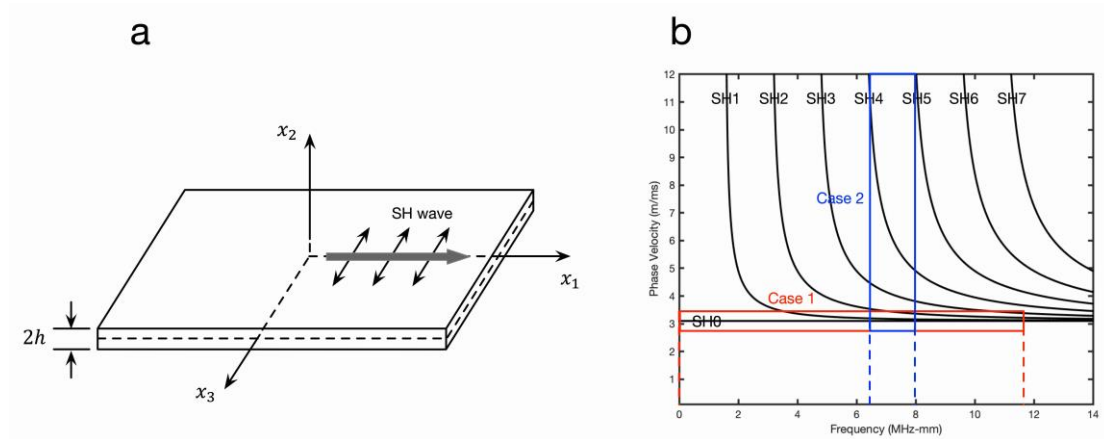


Fig. 1. (a) The SH wave propagation traveling along the x_1 direction and particle displacement u_3 in the axis of x_3 . (b) Dispersion curves of SH waves for an aluminum layer ($c_T = 3.2$ m/ms).

Each mode, when excited, will produce different fields inside the layer i.e., the particle displacements and velocities. Also, the stress and strain fields will vary with the depth inside the layer for each mode. In fact, even the same mode at a different

frequency will cause different distributions of fields^[33]. Therefore, it is desirable to leverage the fusion of multiple modes and multi-frequency scattering information for defect reconstruction as different fields including comprehensive defect-relevant information may exhibit the higher sensitivity to different types and orientations of defects. Even each point on the dispersion curve depicted in Fig.1b can be used for defect detection and reconstruction theoretically, the practicability of inspection should also be considered under the consideration of various situations. For example, a single-mode broadband scattered signal (SH0) with the frequency range of 0 MHz to 11.3 MHz (highlighted in red shown in Fig.1b) may contain sufficient defect-related information for quantitative defect reconstruction using some algorithms such as Fourier transform, while the mode separation would be highly required to obtain such a broadband signal due to the complexity. It is noted that a multi-modes narrowband excitation (highlighted in blue) helps to improve the mode purity and interpretability of the guided wave signals, also performs in a more cost-effective manner as compared to a single-mode broadband scattered signal. Furthermore, the multi-modes narrowband signal enables the high-resolution reconstruction of defects as it naturally encompasses comprehensive defect-related information. However, it is challenging to solve such a multi-frequency, multi-mode inverse scattering problem using conventional model-based reconstruction algorithms such as Fourier transform. Taking into account this situation, a data-driven based deep learning model, which have the ability to efficiently extract the defect features, i.e. flaw-associated information from high dimensional data (multi-frequency, multi-modes scattered signals) has been developed for quantitative defect reconstructions by the mapping of data features to defect shapes, leveraging the power of manifold learning for the extraction of signal distributions from the high dimensional space to the low one.

2.2 Distribution of scattering signals in the manifold/vector space

As discussed above, it is desirable to utilize multi-mode, narrowband scattered signals for quantitative defect reconstruction under the consideration of the practicability and cost of inspection. As the reconstruction technique used in this research establishes a data-driven intelligent network model, it is necessary to perform wave analysis of the multi-mode, narrowband signals for the generation of training datasets from the perspective of data structures.

As shown in Fig.2, a thinning flaw with an arbitrary shape is located at the top surface of the plate. It is assumed that the incident guided wave of the SH0 mode propagates from the left to right side and is reflected back by the thinning part. Thus, the reflected wave containing multi-mode information can be observed at the far field and the displacement field is determined by Eq.(3). Considering the dispersion property of the SH-wave, displacements of the incident SH0 wave (u^{inc}) and reflected n th mode wave, u^{inc} and u^{ref} can be rewritten as

$$u^{\text{inc}} = A_0^{\text{inc}}(\omega_m) f_0(q_0 x_2) e^{i(kx_1 - \omega_m t)} \quad (5a)$$

$$u^{\text{ref}} = A_n^{\text{ref}}(\omega_m) f_n(q_n x_2) e^{i(kx_1 + \omega_m t)} \quad (5b)$$

where ω_m means the circular frequency ($m = 1, 2, 3 \dots$); A_n is the amplitude

coefficient of the n th mode in frequency domain, $q_n = \sqrt{\frac{\omega_m^2}{c_T^2} - k^2}$, and f_n is determined by Eq.6

$$f_n(q_n x_2) = \begin{cases} \cos(q_n x_2) & \text{for } n = 0, 2, 4 \dots \\ \sin(q_n x_2) & \text{for } n = 1, 3, 5 \dots \end{cases} \quad (6)$$

The reflection coefficients $C_n(\omega_m)$ of the n th mode reflected wave are formulated by Eq.7

$$C_n(\omega_m) = A_n^{\text{ref}}(\omega_m) / A_0^{\text{inc}}(\omega_m) \quad (7)$$

The matrix representation of $C_n(\omega_m)$ can be written as

$$\mathbf{C}^{mn} = \begin{bmatrix} C_0(\omega_1) & \dots & C_n(\omega_1) \\ \vdots & \ddots & \vdots \\ C_0(\omega_m) & \dots & C_n(\omega_m) \end{bmatrix} \quad (8)$$

Fig.3 presents the absolute values of the complex-valued reflection coefficients for the first three modes of reflected SH waves, namely, 0th symmetric (SH0), 1st anti-symmetric (SH1) and 1st symmetric (SH2) modes. Three defects including the rectangular(a), V-notch(b) and Gaussian-curved(c) thinning are considered in the wave analysis with the frequency range of 7.5 MHz to 12.5 MHz. Results in Figs. 3d-3f represent the fused reflection coefficients that contain the first three order modes.

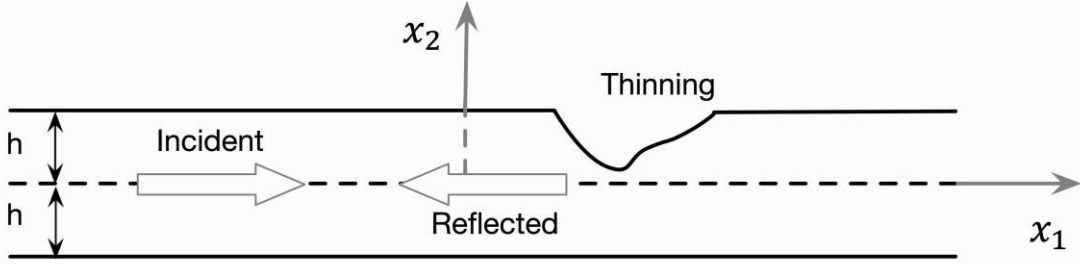


Fig. 2. An incident guided SH-wave is reflected by a plate thinning at the top surface of the plate.

It is worth noting that each complex-valued item $C_n(\omega_m)$ in the matrix \mathbf{C}^{mn} defined in Eq.8 represents the interaction between the sub-waves and the defects in the form of amplitudes and phases of reflection coefficients, which reflect the defect-related information and features. Hence, the procedure for defect reconstruction proposed in this paper is to construct a deep learning operator \mathcal{H} , which has the ability to extract the defect features and further realize the mapping of the reflection coefficients \mathbf{C}^{mn} to the profile of defects \mathbf{D} . It is worth noting that the operator \mathbf{D} is defined by Eq.9

$$\mathbf{D} = \mathcal{H}(\mathbf{C}^{mn}) \quad (9)$$

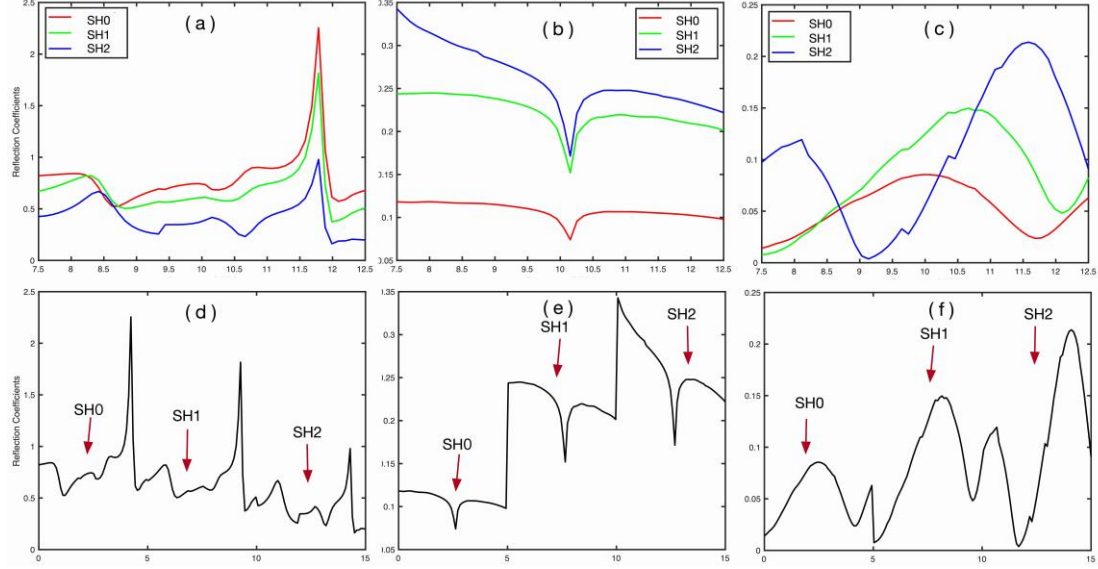


Fig. 3. The absolute value of reflection coefficients for the first three modes of reflected SH-waves. Three defects are considered including the rectangular(a), V-notch(b) and Gaussian-curved thinning (c). (d-f) depict the fused reflection coefficients that contain the first three order modes.

As described in the manifold assumption^[34-35], a natural high-dimensional data distribution concentrates close to a non-linear low-dimensional manifold, and the goal of deep learning aims to learn the manifold structure in data and the probability distribution associated with the manifold. Therefore, if the manifold represented by the scattered data of guided waves i.e., reflection coefficients \mathbf{C}^{mn} , has a simpler, highly separable structure, it would be easier for the deep learning model \mathcal{H} to learn, leading to the higher reconstruction accuracy. Considering this fact, it is necessary to analyze the manifold structure or the vector distribution of reflection coefficients \mathbf{C}^{mn} of guided SH-waves prior to the construction of \mathcal{H} . The t-distributed stochastic neighbor embedding (t-SNE)^[36] is applied to realize a flexible dimension reduction and visualize the high-dimensional data by a complex mapping to reveal structures of datasets at many different scales. In this paper, the dataset of SH-wave reflection coefficients which reflect three types of defect information (rectangular, V-notch and Gaussian-curved flaws) on the manifold space, have been simulated using the modified boundary element method (MBEM)^[37] for the generation of training data and feature extraction.

The effects of different modes and frequency samples on the pattern of reflection coefficients in the reduced space for feature extractions of defects is demonstrated in Fig.4 by the t-SNE technique. It is noted that for the signals excited by the broadband frequency (Figs. 4a, 4c), the datasets of reflection coefficients in both single mode and multi-modes appear highly separable, that is, natural features of the data for the different types of defects tend to be represented into tight and wide separated clusters in the two dimensional space. When the number (5) of frequency samples in Figs. 4b and d is small and insufficient for defect reconstruction, the feature representation by datasets containing multi-mode defect-related information is significantly clear and distinguishable, as more information related to three types of defects are utilized for defect reconstructions. However, no separable clusters of reflection coefficients can

be clearly identified using the single-mode scattered information. Taking into account the features shown in Fig.4 as well as the practicability and cost in the guided wave inspection, the following observations have been achieved as useful guidelines for practical applications:

- (1) Two guidelines relating to the numbers of frequency samples and wave modes during the guided wave inspection can be leveraged for quantitative defect reconstruction as substantial defect information, e.g., reflection coefficients, is contained in the scattered signals.
- (2) To realize a guided wave inverse scattering technique with a high level of accuracy, it is worth noting that the single-mode, broadband scattered signals containing sufficient defect-related information is compulsory. This conclusion is demonstrated by the highly separable dataset in Fig. 4a. However, the mode separation is extremely challenging for a signal with such broadband frequencies. Also, the cost of wave excitation force during the experiment test is increasingly expensive.
- (3) As the defect-related information is insufficient in the single mode signal with narrowband frequencies, the results represented in the lower-dimensional space indicate poorly separable in Fig. 4b. Based on this observation, it is necessary to utilize the multi-modes, narrowband signal that encompasses comprehensive defect-related information for defect reconstruction economically.
- (4) Constructing defects in use of multi-mode, narrowband signals indeed demonstrates the superior performance as the dataset appears highly separable in Fig. 4d, leading to the development of a more practical and cost-effective defect reconstruction technique. Therefore, deep learning models have to be developed to solve such a multi-frequency, multi-modes problem which is challenging for conventional model-based reconstruction algorithm.

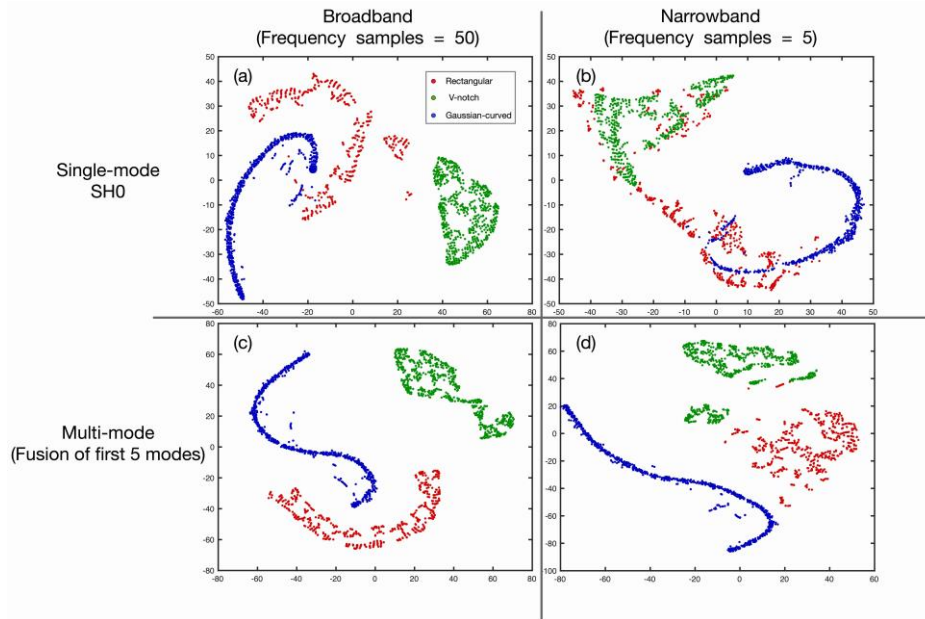


Fig. 4. t-SNE visualization of scattered signals (reflection coefficients) under different cases of wave modes and frequency band.

2.3 The proposed encoder-projection-decoder architecture

To intelligently realize the end-to-end mapping between the multi-frequency, multi-mode guided wave scattered signals and defect profiles with high levels of accuracy and efficiency, a novel encoder-projection-decoder neural network has been proposed to leverage the mechanism of the manifold distribution principle, leading to the facilitation of defect feature extractions in the low-dimensional space. The overall architecture of the proposed neural network is depicted in Fig. 5. As the developed computational framework operates on real-valued inputs, it is noted that the reflection coefficients or experimental data must be divided into two groups storing the real and imaginary components concatenated into the input vector. For example, a $m \times n$ complex-valued reflection coefficient matrix should be reshaped to a $2mn \times 1$ real-valued vector (m means the number of frequency samples and n depicts the number of modes). In this study, the size of 144×1 for the output in spatial space is predefined. Following that, the encoder part converts the input into the data represented in a squeezed dimension in a manner similar to general CNNs. This process consists of sequential blocks of convolutions with a stride of 2 and a factor of 2, leading to the increase of the number of feature layers. Then, the batch normalization (BN) and activation by a rectified linear unit (ReLU) are applied before the projection part. It is worth noting that the convolution filter size of 3×1 is used throughout the encoder, in which there are 32 feature maps with the dimension of $mn \times 1$ included. Each feature is represented by a non-linear function of an extensive portion of the input reflection coefficients.

To facilitate the feature extraction related to the input data, i.e., reflection coefficients from a high-dimensional space to a homeomorphic representation, the latent projection is implemented as an operator to highlight the features of defect profiles. As schematically illustrated in Fig. 5, the first layer of the projection is fully connected to an 72×1 -dimensional hidden layer with the hyperbolic tangent activation. Once the features are projected into a manifold space, the decoder part upsamples the main defect features represented by the latent projection to finalize the profiles of defects as the output in a spacial space. In the decoder process, each step along the path increasing the data interpretability consists of a 3×1 deconvolution layer that halves the number of feature layers and a BN layer followed by a ReLU activation. The total number of convolutional layers in the whole encoder-projection-decoder network is set to 8.

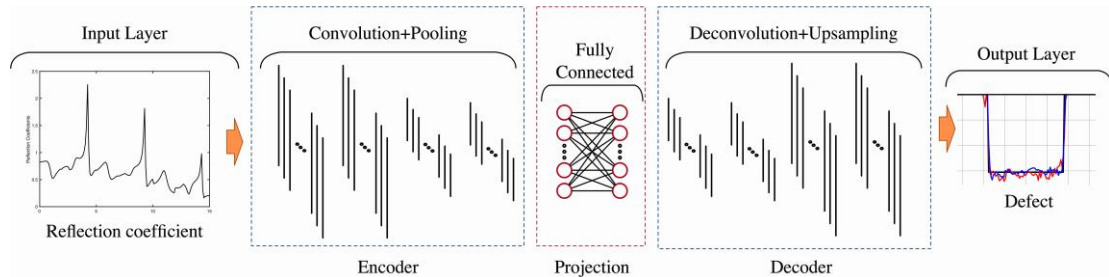


Fig. 5. The overall schematic architecture of the proposed encoder-projection-decoder neural network for quantitative structural defect reconstruction.

2.4 Dataset generation

To obtain the training data for the proposed network, reconstructions of surface thinning flaws in a 2-dimensional steel plate shown in Fig. 2 using guided SH-wave is performed. The capability of the proposed encoder-projection-decoder neural network to quantitatively reconstruct defect profiles is demonstrated with the fusion of multi-frequency, multi-mode information encompassed in scattered signals throughout the examples. The material properties of the steel plate is listed in Table 1.

Table 1 The material properties of the steel plate.

Material	Young modulus (Gpa)	Poisson	Density (kg/m ³)	Plate thickness (mm)
Steel	207.18	0.2949	7800	1

In order to efficiently generate sufficient data for the exploration of defect features via the powerful data-mining capability of the Deep-guide framework, the modified boundary element method (MBEM)^[37] is applied to calculate reflection coefficients of guided waves propagating through the plate with thinning defects. The implementation of MBEM not only aims at obtaining the input data by performing the ultrasonic guided wave analysis, but provides an insight to the development of physics-informed network by the fusion of numerical results or experimental data containing multi-frequency, multi-wave-mode information and the data-driven manifold learning technique for quantitatively solving the guided wave inverse scattering problems in the field of nondestructive evaluation.

In this research, a dataset of 4000 scattered signals (reflection coefficients) from four typical shapes of surface defects including the rectangular, V-notch, Gaussian-curved and double rectangular flaws in plates, have been obtained using MBEM. Numerical simulations of 4000 plate thinning defects using the SH₀ guided wave mode have been performed to obtain reflection coefficients, which are used as the inputs for training the proposed network. Results in these 4000 cases have been treated as the ground truth. The circular frequency ω takes the value from the range of 0.1 MHz to 14.0 MHz with the increment of 0.1, and therefore a total of 140 frequency samples have been considered. The amplitude coefficients of the first five SH-wave modes have been obtained at each frequency sample. The use of the training data for the reconstruction of defects by the proposed method is discussed with more details in Section 3.

2.5 Network training and quality evaluation of defect reconstruction

To effectively train the proposed network, the dataset has been randomly divided into three splits. Out of the total 4000 samples, 2800 data have been used for network training (70%), 600 for the validation (15%), and 600 for testing (15%).

The proposed network has been initially implemented in Tensorflow^[38], and then trained and tested on a NVIDIA 3080 graphics processing units (GPUs). The mean squared error (MSE) between the network output and ground truth data has been used

as the loss function defined by Eq.9

$$\text{MSE} = \frac{1}{n} \sum_{i=1}^n (x_i - y_i)^2 \quad (10)$$

where x is the reconstructed defect, y is the ground truth, and n is the number of defect pixels. The Adam optimization method has been selected to achieve the converged results. Once the network training followed by the validation process is completed, the correctness and robustness of the network model with optimal performances will be evaluated by the test set.

For the quality evaluation of defect reconstruction, two metrics have been considered to assess the superior performance of the proposed network over the other existing methods. The first criterion is the root mean square error (RMSE) formulated as:

$$\text{RMSE} = \sqrt{\frac{\sum_{i=1}^N (x_i - \hat{x}_i)^2}{N}} \quad (11)$$

where N is the number of pixels; x_i is the pixel value of the ground truth and \hat{x}_i is the pixel value of the reconstructed defect. The lower RMSE value means the better accuracy of the reconstructed defect profiles.

The second metrics used for the defect quality evaluation is the peak signal-to-noise ratio (PSNR) defined by Eq.11:

$$\text{PSNR} = 20 \cdot \log_{10} \left(\frac{x_{\max}}{\text{RMSE}} \right) \quad (12)$$

where x_{\max} is the maximal pixel value of the ground truth x . A higher value of PSNR represents the better defect quality.

3. Numerical validation

3.1 Validation of the proposed method

To validate the correctness and effectiveness of the proposed deep learning-based quantitative inverse scattering method, the novel encoder-projection-decoder neural network enabling the manifold learning capability has been trained using the multi-frequency, multi-modes scattered signals, which have been obtained by MBEM simulations^[36]. It should be noted that frequencies of the scattered signals used in this study has been in the range of 7MHz to 12MHz with the increment of 0.1, a total of 50 frequency samples. Following that, the unknown defects in the test set have been reconstructed using the trained network. It is worth noting that the same network architecture and hyper-parameters have been kept intact during the process of defect reconstructions for different inputs so that the generalization of the developed deep learning network can be evaluated.

The reconstructed defects with three types of profiles (Rectangular, V-notch and Gaussian-curved defects) using different modes of SH-waves (SH0, SH1, SH2, the fusion of first 3 modes and the fusion of first 5 modes) have been provided in Fig.6. It can be observed that main features of the defects have been successfully reconstructed in all three cases, where the remarkable capability of the proposed data-driven method for defect reconstruction using multiple modes, multi-frequency scattered signals has been demonstrated. Moreover, the advantage of the proposed deep learning network

has been evidenced by less than 0.1 seconds of computational time for defect reconstruction as the framework has only requires one pass to execute calculations.

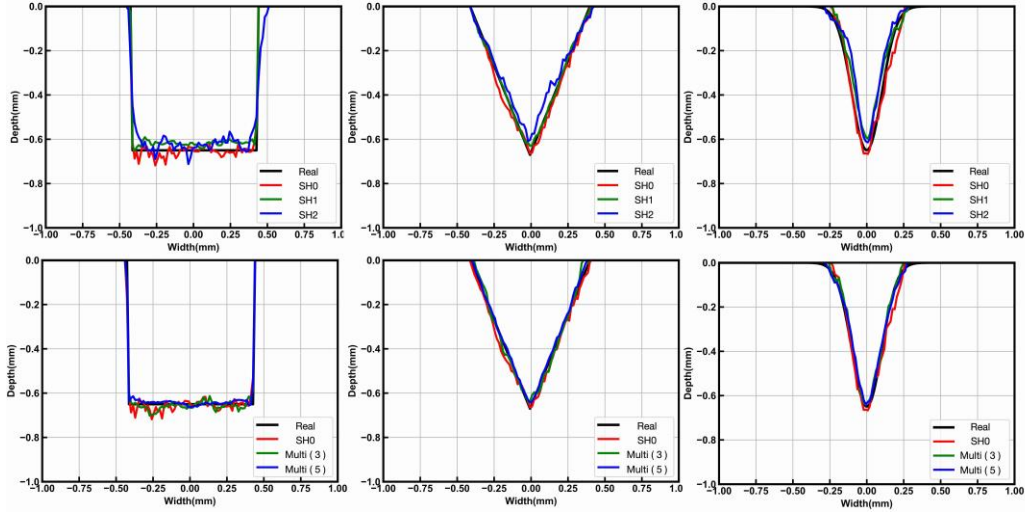


Fig. 6. Reconstruction results of plate surface defects using the encoder-projection-decoder neural network (plate thickness $h = 1mm$).

Furthermore, the quantitative evaluations on the quality of reconstructions by the average RMSE and PSNR over the entire test set (600 samples) have been provided in Tables 2. It has been observed that the lowest average RMSE (0.0166) among the reconstruction results in all three cases has been achieved using the fusion of first 5 modes, as compared with 0.0212 by the fusion of first 3 modes (27.71% higher), 0.0252 by the SH0 mode (51.82% higher), 0.0298 by the SH1 mode (79.52% higher) and 0.0485 by the SH2 mode (175.90%). The similar conclusion can be drawn for the quality evaluation of reconstruction results by the average PSNR, that is to say, the best result of 28.95dB by the fusion of first 5 modes can be identified, whilst 26.84dB (2.11dB lower) the fusion of first 3 modes, 25.30dB (3.65dB lower) for the SH0 mode, 23.39dB (5.56dB lower) for the SH1 mode and 19.39dB (9.56dB lower) for the SH2 mode.

It is also worth noting that the V-notch defect reconstruction has been realized for the best precision with the average RMSE of 0.0229, which has been improved by 34.06% and 28.82% from 0.0307 and 0.0295 for the rectangular and Gaussian-curved reconstructions, respectively. This can be interpreted from the perspective of manifold analysis illustrated in Section 2.2: the higher separable pattern represented by green dots in Fig. 4 indicates the manifold of scattered signals by V-notch defects, as compared with the manifolds by the other two types of defects.

Table 2 RMSE and PSNR of reconstructed defect shapes.

Case	Defects	Rectangular	V-notch	Gaussian-curved	Average
		SH0	RMSE 0.0279	0.0224	0.0253
	PSNR(dB)	24.07	26.73	25.09	25.30
SH1	RMSE	0.0284	0.0229	0.0381	0.0298

	PSNR(dB)	23.84	25.52	20.83	23.39
SH2	RMSE	0.0571	0.0332	0.0471	0.0458
	PSNR(dB)	16.92	22.51	18.75	19.39
Fusion of first 3 modes	RMSE	0.0221	0.0213	0.0201	0.0212
	PSNR(dB)	25.54	27.29	27.68	26.84
Fusion of first 5 modes	RMSE	0.0182	0.0149	0.0167	0.0166
	PSNR(dB)	26.82	31.59	28.45	28.95
Average	RMSE	0.0307	0.0229	0.0295	
	PSNR(dB)	23.44	26.73	24.16	

In Fig. 7, boxplots of reconstruction results using multiple modes information of the scattered SH-waves have been presented to demonstrate the high precision of the proposed technique. It can be observed that the deep learning-based quantitative guided wave inverse scattering approach leveraging the multi-modes information has the ability to achieve a high level of stability, leading to a relatively narrower distribution of RMSE over the entire test dataset, whereas results reflecting the poorer stability on a wider range of RMSE can be identified given the information from single-mode scattered signals for reconstructions. The minimum median value (0.0139) has indicated the superiority of the proposed approach to defect reconstructions using the fusion of the first 5 modes over one single mode or few fused modes in terms of accuracy, for example, the reconstruction RMSE of 0.0204 (46.76% higher) by the single SH0 mode.

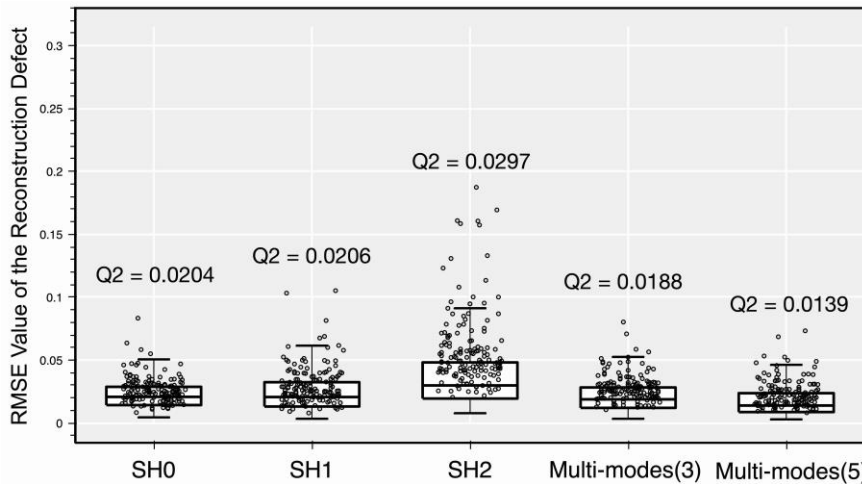


Fig. 7. Quantitative evaluations on the quality of reconstruction with RMSE over the entire 600 test data which include three types of unknown defects. The x axis represents the wave modes used for reconstruction. The y axis denotes the values of RMSE between the reconstructed defects and the ground truth. Each box shows the interquartile range (IQR between Q1 and Q3) of the test results. The central mark (the horizontal line in each box) shows the median value Q2. The upper whisker extends from the hinge to the largest value no further than $Q3+1.5 \times IQR$ and the lower whisker extends from the hinge to the smallest value at most $Q1-1.5 \times IQR$. For each box, 150 values randomly selected from the 600 test results are shown as dots.

3.2 Defect reconstruction by narrowband signals

As described in Section 2.2, it is extremely challenging to achieve the mode separation for a scattered signal in broadband frequencies and also increasingly expensive to excite ultrasonic guided waves at different frequencies. Therefore, the motivation of this research is to investigate the reconstruction performance of the proposed technique using the scattered signals that occupy the narrowband frequencies. Fig. 10 has shown the comparison of the reconstructed results using different numbers of frequency samples with the real defects. As the defect-related information is insufficient for defect reconstruction by the single mode signal in narrowband frequencies, it has been concluded that the fewer the number of frequency samples for defect reconstruction is, the poorer the quality of reconstruction by a single mode of SH0 performs.

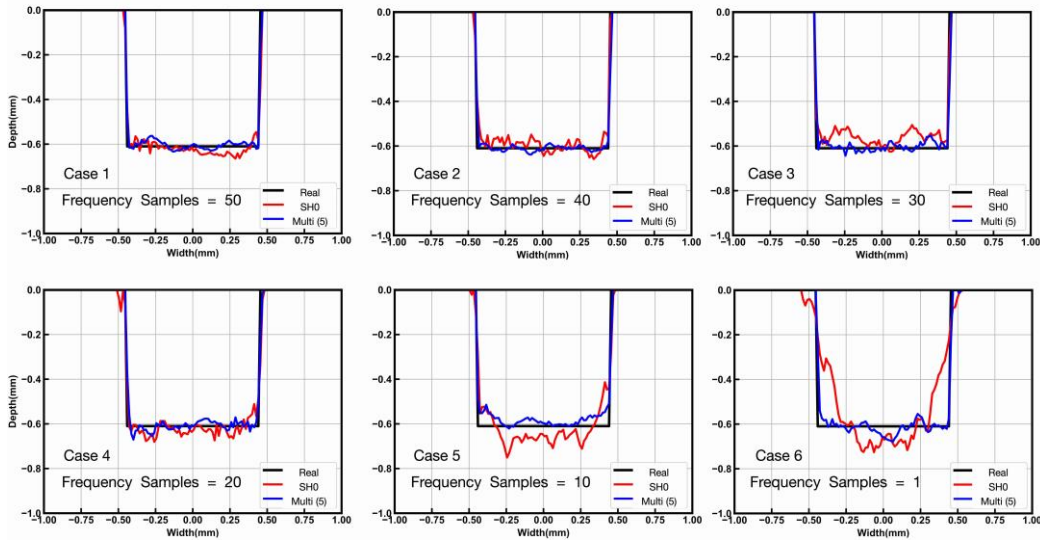


Fig.8. Defect reconstruction using different numbers of frequency samples.

Moreover, the quantitative evaluations on the quality of reconstructions using different numbers of frequency samples have been provided in Table 3. It can be observed that as the number of frequency samples has decreased, results of defect reconstructions using the single mode and multi-modes scattered signals have become poorer. However, the overall performance of reconstruction using the multi-modes signals is relatively better and more stable as compared with the reconstructions by the single mode signal. For example, the reconstruction using the fusion of the first 5 modes with 50 frequency samples has demonstrated the best accuracy with the lowest average RMSE (0.0225) and the highest average PSNR (28.65dB). Furthermore, for the defect reconstruction using only one frequency sample, the result obtained by the fusion of first 5 modes signals still has more trustworthy accuracy with the average RMSE value of 0.0389, as compared with 0.1062 (173.01% lower) predicted by the model using the SH0 signal.

Table 3 The quantitative evaluation of reconstruction results using models trained with different numbers of frequency samples.

		50	40	30	20	10	1
SH0	RMSE	0.0376	0.0303	0.0402	0.0409	0.0601	0.1062
	PSNR(d)	24.19	26.07	23.62	23.48	20.12	15.19
	B)						
Fusion of first 5 modes	RMSE	0.0225	0.0284	0.0352	0.0324	0.0320	0.0389
	PSNR(d)	28.65	26.63	24.77	25.49	25.60	23.91
	B)						

A more direct quantitative comparison of the reconstruction qualities using the single-mode and multi-modes scattered signals has been shown in Fig.9. It is worth noting that the reconstruction using the multi-modes scattered signals, e.g., the green line and blue line, can still achieve high levels of precision by models trained with a few of frequency samples. For example, the reconstruction using the SH0 mode requires 50 frequency samples to achieve the RMSE value of 0.024 or PSNR value of 24.83dB, while only about 25 frequency samples are used for the reconstruction by the fusion of the first 5 modes for the same level of accuracy. Also, for reconstruction using a single mode scattered signal, the precision decreases rapidly as the number of frequency samples decreases, while the accuracy is reduced slightly for the reconstruction by the fuse of multi-modes information.

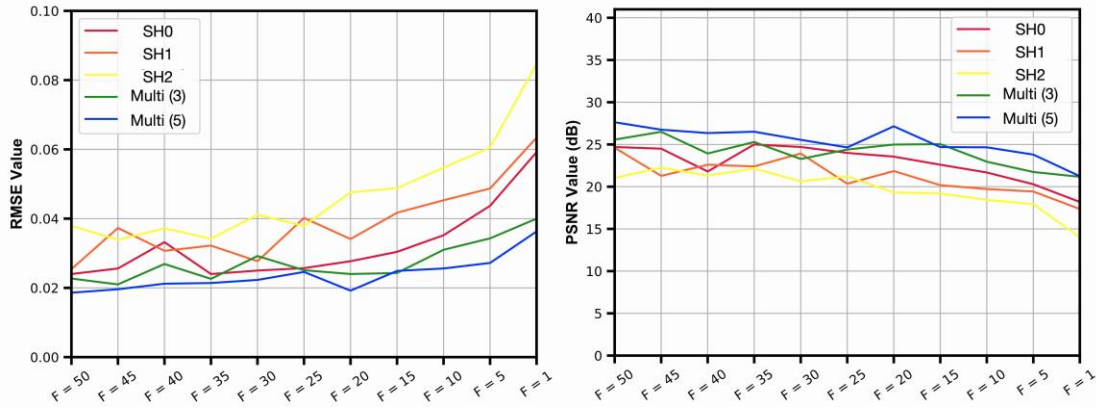


Fig.9. Comparison of the reconstruction precision on the entire test set from models trained with different numbers of frequency samples in different scenarios.

3.3 Comparison with the Fourier transform reconstruction

In this section, a state-of-art conventional knowledge-driven reconstruction method, which is called Born approximation-based Fourier transform (BFT) has been compared against the proposed data-driven deep learning method (DDDL) in terms of defect reconstruction performance. The double-notch defect reconstruction results have been shown in Fig. 10 and the quantitative evaluation on the quality have been provided in Table 4. It has been noted that the frequency range of the scattered signals used in the BFT reconstruction has been set from 0MHz to 14MHz including 140 frequency

samples, while only 32 frequency samples in the range of 6.3MHz to 7.9MHz have been used in DDDL. It can be observed that the defect reconstruction by DDDL with the fusion of the first 5 SH-waves modes has shown better quality with the lowest average value (0.0475) of RMSE and the highest average value (22.84dB) of PSNR, as compared with 0.0547 (15.16% higher) and 19.63dB (3.21dB lower) by BFT, 0.0725 (52.63% higher) and 9.77dB (13.07dB lower) by DDDL using the single mode (SH0) scattered signal. As sufficient frequency samples have been provided in the comparison study, the FT method could also produce results with a relatively trustworthy reconstruction quality. The reason for this observation has been provided in Section 2.2. Considering the challenge of the mode separation for such a broadband frequencies signals and the increasingly expensive cost of wave excitation, the proposed deep learning-based method has the ability to efficiently achieve the high-quality defect reconstructions using fewer frequency samples, enabling the development of practical techniques for quantitative ultrasonic guided wave inspection using multi-frequency and multi-mode acoustic data.

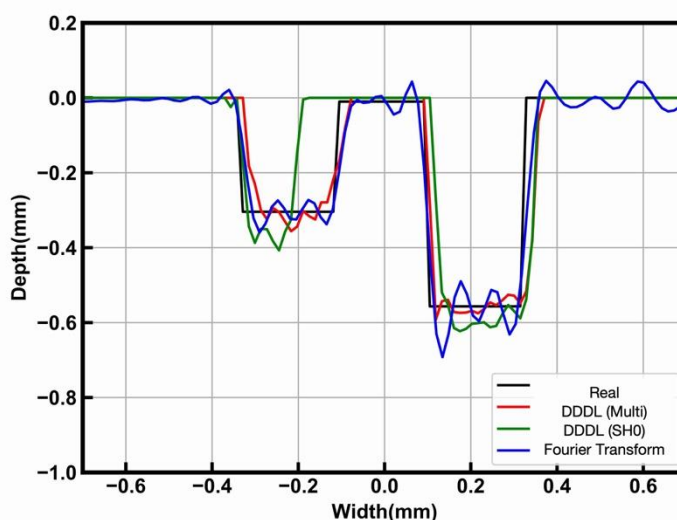


Fig.10. Comparison of reconstruction results from different techniques.

Table 4 The quantitative evaluation of reconstruction results from different techniques.

	DDDL (Fusion of 5 modes)	DDDL (Single SH0 mode)	Fourier transform(FT)
RMSE	0.0475	0.0725	0.0547
PSNR(dB)	22.84	9.77	19.63

4. Conclusion

In this paper, a novel deep learning-based guided wave inverse scattering technique for quantitative structural defect reconstructions has been proposed to automatically realize the end-to-end mapping of the multi-frequency, multi-modes scattered ultrasonic guided wave signals to defect profiles with high levels of accuracy and efficiency. Based on the manifold distribution principle of the acoustic data, the encoder-

projection-decoder network has been trained by multi-frequency, multi-modes scattered signals to enhance the manifold-learning capability. To further demonstrate the correctness and effectiveness of the proposed defect reconstruction technique, numerical validations in different scenarios have been performed with the main conclusions as follows:

- (1) Defect reconstruction using the scattered ultrasonic signals with the fusion of different wave modes has achieved high levels of accuracy and efficiency, for example, the RMSE values of reconstruction results by the fusion of first 5 modes, the fusion of first 3 modes, the SH0 mode, the SH1 mode and the SH2 mode have been obtained as 0.0166, 0.0212, 0.0252, 0.0298 and 0.0485, respectively.
- (2) Multi-modes narrowband scattered signals have enabled the higher resolution reconstruction of defects and also performed in a more practical and cost-effective manner as compared with the results by broadband scattered signals.
- (3) The superiority of the proposed data-driven technique over traditional knowledge-driven reconstruction approaches has been clearly demonstrated by the effective defect reconstructs using fewer frequency samples.

Summarily, using the fusion of multi-modes and multi-frequency defect-related information has enabled defect reconstructions with high levels of accuracy and reliability, and also provided a useful insight into the development of practical quantitative end-to-end inverse scattering techniques for the inspection and reconstruction of complex defects using ultrasonic guided waves.

Declaration of Competing Interest

None.

Acknowledgments

This work is supported by the National Natural Science Foundation of China (12061131013, 12211530064 and 12172171), the State Key Laboratory of Mechanics and Control of Mechanical Structures at NUAU (No. MCMS-E-0520K02), the Fundamental Research Funds for the Central Universities (Nos. NE2020002 and NS2019007), the National Natural Science Foundation of China for Creative Research Groups (No. 51921003), Postgraduate Research & Practice Innovation Program of Jiangsu Province (No. KYCX21_0184), the National Natural Science Foundation of Jiangsu Province (No. BK20211176), the Interdisciplinary Innovation Fund for Doctoral Students of Nanjing University of Aeronautics and Astronautics [grant number KXKCXJJ202208 and a project funded by the Priority Academic Program Development of Jiangsu Higher Education Institutions (PAPD)].

Corresponding authors

Correspondence to dianzi.liu@uea.ac.uk and qianzh@nuaa.edu.cn

Availability of data and materials

The data that support the findings of this study are available on request from the corresponding author.

References

- [1] Rose J L 2002 A Baseline and Vision of Ultrasonic Guided Wave Inspection Potential *Journal of pressure vessel technology* 124(3):273-82
- [2] Olisa S C, Khan M A and Starr A 2021 Review of current guided wave ultrasonic testing (GWUT) limitations and future directions *Sensors (Basel, Switzerland)*. 21(3):1-28
- [3] Wang X, Tse P W, Mechefske C K and Hua M 2010 Experimental investigation of reflection in guided wave-based inspection for the characterization of pipeline defects *NDT & E international : independent nondestructive testing and evaluation* 43(4):365-74
- [4] Jin H, Yan J, Liu X, Li W and Qing X 2021 Quantitative defect inspection in the curved composite structure using the modified probabilistic tomography algorithm and fusion of damage index *Ultrasonics*. 113:106358
- [5] Leonard K R, Malyarenko E V and Hinders MK 2002 Ultrasonic Lamb wave tomography *Inverse problems*. 18(6):1795-808
- [6] Arridge S, Maass P, Öktem O and Schönlieb C B 2019 Solving inverse problems using data-driven models *Acta numerica*. 28:1-174
- [7] Poudel J and Anastasio M A 2020 Joint reconstruction of initial pressure distribution and spatial distribution of acoustic properties of elastic media with application to transcranial photoacoustic tomography *Inverse Problems*. 36(12), 124007
- [8] Drinkwater B W and Wilcox P D 2006 Ultrasonic arrays for non-destructive evaluation: A review *NDT & E international : independent nondestructive testing and evaluation*. 39(7):525-41
- [9] Jansen D P, Hutchins D A and Mottram JT 1994 Lamb wave tomography of advanced composite laminates containing damage *Ultrasonics*. 32(2):83-90
- [10] Wright W, Hutchins D, Jansen D and Schindel D 1997 Air-coupled Lamb wave tomography *IEEE transactions on ultrasonics, ferroelectrics, and frequency control*. 44(1):53-9
- [11] Nagata Y, Huang J, Achenbach J D and Krishnaswamy S 1994 LAMB WAVE TOMOGRAPHY USING LASER-BASED ULTRASONICS *Annual Review of Progress in Quantitative Nondestructive Evaluation*. Jul 31-Aug 04
- [12] Levent D F, Pei J, Khuri-Yakub B T and Saraswat K C 1994 In situ acoustic temperature tomography of semiconductor wafers *Applied physics letters*. 64(11):1338-40
- [13] McKeon J C P and Hinders M K 1999 Parallel projection and crosshole Lamb wave contact scanning tomography *The Journal of the Acoustical Society of America*. 106(5):2568-77
- [14] Malyarenko E V and Hinders M K 2001 Ultrasonic Lamb wave diffraction tomography *Ultrasonics*. 39(4):269-81
- [15] Hay T R, Royer R L, Gao H, Zhao X and Rose J L 2006 A comparison of embedded sensor Lamb wave ultrasonic tomography approaches for material loss detection *Smart materials and structures*. 15(4):946-51
- [16] Koduru J P and Rose J L 2013 Mode controlled guided wave tomography using annular array transducers for SHM of water loaded plate like structures *Smart materials and structures*. 22(12):125021

- [17] Lee J, Sheen B and Cho Y 2015 Quantitative tomographic visualization for irregular shape defects by guided wave long range inspection *International journal of precision engineering and manufacturing*. 16(9):1949-54
- [18] Li X, Guo W, Li X, Zhang Z and Liu Y 2017 Ultrasonic Guided Wave Scattering Matrices and Tomography Using Sparse Arrays for Defect Characterization *International Conference on Sensing, Diagnostics, Prognostics, and Control (SDPC)*. IEEE. 688-693
- [19] Zhang K and Zhou Z 2018 Quantitative characterization of disbonds in multilayered bonded composites using laser ultrasonic guided waves *NDT & E international : independent nondestructive testing and evaluation*. 97:42-50
- [20] Wang B and Hirose S 2012 Inverse Problem for Shape Reconstruction of Plate-Thinning by Guided SH-Waves *Materials transactions*. 53(10):1782-9
- [21] Wang B and Hirose S 2012 Shape Reconstruction of Plate Thinning Using Reflection Coefficients of Ultrasonic Lamb Waves: a Numerical Approach *ISIJ international*. 52(7):1320-7
- [22] Jarmer G J S, Flynn E B and Todd MD 2014 Multi-wave-mode, multi-frequency detectors for guided wave interrogation of plate structures *Structural health monitoring*. 13(2):120-30
- [23] Juarez P D and Leckey C A C 2015 Multi-frequency local wavenumber analysis and ply correlation of delamination damage *Ultrasonics*. 62:56-65
- [24] Michaels J E, Lee S J, Hall J S and Michaels T E 2011 Multi-mode and multi-frequency guided wave imaging via chirp excitations *Proceedings of SPIE, the International Society for Optical Engineering*. Bellingham WA: SPIE. 7984
- [25] Da Y, Dong G, Wang B, Liu D and Qian Z 2018 A novel approach to surface defect detection *International journal of engineering science*. 133:181-95
- [26] Pereira D and Belanger P 2019 Inverse characterization of adhesive shear modulus in bonded stiffeners using ultrasonic guided waves *AIP Conference Proceedings*. 2102(1)
- [27] Gao T, Sun H, Hong Y and Qing X 2020 Hidden corrosion detection using laser ultrasonic guided waves with multi-frequency local wavenumber estimation *Ultrasonics*. 108:106182-
- [28] Sun Y, Xia Z and Kamilov U S 2018 Efficient and accurate inversion of multiple scattering with deep learning *Optics express*. 26(11):14678-88
- [29] Chen H, Zhang Y, Kalra M K, Lin F, Chen Y, Liao P 2017 Low-Dose CT With a Residual Encoder-Decoder Convolutional Neural Network *IEEE transactions on medical imaging*. 36(12):2524-2535
- [30] Zhu B, Liu J Z, Cauley S F, Rosen B R and Rosen M S 2018 Image reconstruction by domain-transform manifold learning *Nature (London)*. 555(7697):487-92
- [31] Häggström I, Schmidlein C R, Campanella G and Fuchs T J 2019 DeepPET: A deep encoder-decoder network for directly solving the PET image reconstruction inverse problem *Medical image analysis*. 54:253-62
- [32] Melville J, Alguri K S, Deemer C, Harley J B 2017 Structural Damage Detection Using Deep Learning of Ultrasonic Guided Waves *44th Annual Conference on Review of Progress in Quantitative Nondestructive Evaluation (QNDE)*. Jul 16-21; Provo, UT2018
- [33] Jarmer G J, Flynn E B, Todd MD 2014 Multi-wave-mode, multi-frequency detectors for guided wave interrogation of plate structures *Structural Health Monitoring*. 13(2), 120-130
- [34] Tenenbaum J B, De Silva V, Langford J C 2000 A global geometric framework for nonlinear dimensionality reduction *Science (American Association for the Advancement of Science)*. 290(5500), 2319-2323

- [35] Lei N, An D, Guo Y, Su K, Liu S, Luo Z, Yau S and Gu X 2020 A geometric understanding of deep learning *Engineering (Beijing, China)*. 6(3), 361-374
- [36] Van D, Maaten L and Hinton G 2018 Visualizing data using t-SNE *Journal of Machine Learning Research*. 9, 2579-2625
- [37] Yang C, Wang B and Qian Z 2021 Three dimensional modified BEM analysis of forward scattering problems in elastic solids *Engineering analysis with boundary elements* 122:145-54
- [38] Abadi M, Agarwal A, Barham P, Brevdo, E, Chen Z, Citro C and Zheng X 2016 Tensorflow: Large-scale machine learning on heterogeneous distributed systems *arXiv preprint*. arXiv:1603.04467